CHEMISTRY OF MATERIALS
Article

Chem. Mater. **2009,** *21,* 2957–2966 2957
DOI:10.1021/cm9006876

$LaSr_2AlO_5$, a Versatile Host Compound for Ce^{3+}-Based Yellow Phosphors: Structural Tuning of Optical Properties and Use in Solid-State White Lighting

Won Bin Im,*,† Natalie N. Fellows,† Steven P. DenBaars,† Ram Seshadri,† and Young-Il Kim‡

†*Solid State Lighting & Energy Center and Materials Department, University of California, Santa Barbara, California 93106, and* ‡*Department of Chemistry, Yeungnam University, Gyeongsan, Gyeongbuk 712-749, Republic of Korea*

Received March 10, 2009. Revised Manuscript Received April 21, 2009

Cerium-doped lanthanum strontium aluminum oxide $LaSr_2AlO_5:Ce^{3+}$ has recently been identified by us as a viable yellow phosphor that in conjunction with a blue-emitting diode can be used in solid-state white lighting sources. In this study, we present the energy level structure relevant to the luminescence process within $LaSr_2AlO_5:Ce^{3+}$, based on crystal structure determination by powder X-ray diffraction and the peak deconvolution of excitation and emission spectra. We also establish the versatility of the phosphor host $LaSr_2AlO_5$ by examining isovalent substitutions of all three cation types in the structure; Gd or Tb for La, Ca or Ba for Sr, and B or Ga for Al. All the above cation substitutions/solid solution are achieved to the full extent except when Ca (for Sr) or B (for Al) are chosen as substituent. Optical properties of the prepared Ce^{3+} phosphors are found to depend on the rare-earth metal−oxygen distances and the lattice ionicity. Among the compounds studied here, excitation maxima range between 435 and 453 nm and emission maxima between 552 and 577 nm, which are promising for delicate color control in InGaN-based blue-pumped, yellow-emitting phosphors for solid-state white lighting. Prototype light-emitting diodes have been fabricated by formulating various phosphor compositions obtained in this study, and their electroluminescence properties are presented.

Introduction

The past decade has seen a rapid evolution of the GaN-based light-emitting diode (LED) technology, specifically focused on developing advanced solid-state lighting sources.[1,2] Compared with the incandescent or fluorescent lamps, LED-based lighting can provide significant power saving, higher luminous efficiency, longer lifetime, etc. For generating white light, most current commercial LED lamps employ yellow-emitting $Y_3Al_5O_{12}:Ce^{3+}$ ($YAG:Ce^{3+}$) phosphors excited by blue InGaN diodes due to the unsurpassed efficiency such a combination provides.[3−5] However, $YAG:Ce^{3+}$ phosphors have relatively weak emission in the red spectral region, and consequently the color rendering ability has yet to be improved.[6−8] In addition, the output color from $YAG:Ce^{3+}$ phosphors is strongly dependent on temperature and current, which will become a significant problem in high-power LEDs.[9] To overcome these drawbacks, and to avoid issues associated with intellectual property, there are extensive efforts worldwide to develop new yellow-emitting phosphors for blue-pumped LED applications,[10−12] as well as to optimize the existing systems.[6,14]

Recently, we reported a new yellow-emitting phosphor $LaSr_2AlO_5:Ce^{3+}$, potentially applicable to white LED assemblies.[13] Optimally doped $LaSr_2AlO_5:Ce^{3+}$ exhibits an absorption band in the sub-blue region along with strong yellow emission centered at 556 nm, which makes it a favorable candidate for the phosphor component of InGaN-based LED lamps. The quaternary host $LaSr_2AlO_5$ is isostructural with $EuSr_2AlO_5$,[17] in which the rare-earth cation is surrounded by eight

*Corresponding author. E-mail: imwonbin@mrl.ucsb.edu.

(1) Nakamura, S.; Mukai, T.; Senoh, M. *Appl. Phys. Lett.* **1994**, *64*, 1687.
(2) Hashimoto, T.; Wu, F.; Speck, J. S.; Nakamura, S. *Nat. Mater.* **2007**, *6*, 568.
(3) Haranath, D.; Chander, H.; Sharma, P.; Singh, S. *Appl. Phys. Lett.* **2006**, *89*, 173118.
(4) Lu, C.-H.; Jagannathan, R. *Appl. Phys. Lett.* **2002**, *80*, 3608.
(5) Kasuya, R.; Kawano, A.; Isobe, T.; Kuma, H.; Katano, J. *Appl. Phys. Lett.* **2007**, *91*, 111916.
(6) Jang, H. S.; Im, W. B.; Lee, D. C.; Jeon, D. Y.; Kim, S. S. *J. Lumin.* **2007**, *126*, 371.
(7) Chen, Y.; Gong, M.; Wang, G.; Su, Q. *Appl. Phys. Lett.* **2007**, *91*, 071117.
(8) Xie, R.-J.; Hirosaki, N.; Sakuma, K.; Yamamoto, Y.; Mitomo, M. *Appl. Phys. Lett.* **2004**, *84*, 5404.
(9) Piao, X.; Machida, K. I.; Horikawa, T.; Hanzawa, H.; Shimomura, Y.; Kijima, N. *Chem. Mater.* **2007**, *19*, 4592.
(10) Park, J. K.; Lim, M. A.; Kim, C. H.; Park, H. D.; Park, J. T.; Choi, S. Y. *Appl. Phys. Lett.* **2003**, *82*, 683.
(11) Li, Y. Q.; Delsing, A. C. A.; de With, G.; Hintzen, H. T. *Chem. Mater.* **2005**, *17*, 3242.
(12) Saradhi, M. P.; Varadaraju, U. V. *Chem. Mater.* **2006**, *18*, 5267.
(13) Im, W. B.; Kim, Y.-I.; Fellows, N. N.; Masui, H.; Hirata, G. A.; DenBaars, S. P.; Seshadri, R. *Appl. Phys. Lett.* **2008**, *93*, 091905.

Published on Web 05/22/2009

Table 1. Ionic Radii (Å) for the Given Coordination Number (CN)

CN = 8		CN = 10		CN = 4	
La^{3+}	1.160	Ba^{2+}	1.52	Ga^{3+}	0.47
Ce^{3+}	1.143	Sr^{2+}	1.36	Al^{3+}	0.39
Gd^{3+}	1.053	Ca^{2+}	1.23	B^{3+}	0.11
Tb^{3+}	1.040				
Ba^{2+}	1.42				
Sr^{2+}	1.26				
Ca^{2+}	1.12				

oxygen atoms to have the site symmetry of *m*2*m*. Although $EuSr_2AlO_5$ is somewhat similar, both structurally and compositionally with known phosphor hosts, there has been no reported study on this phosphor system prior to our previous note.[13] In this work, we describe the detailed crystal structure of $LaSr_2AlO_5:Ce^{3+}$ as obtained from Rietveld analysis of powder X-ray diffraction patterns, and use the structural information in conjunction with optical measurements to propose the crystal field splitting scheme for the Ce 5d levels in this class of compounds. Density functional calculations, performed using the experimental crystal structure of $LaSr_2AlO_5$, allow features of the electronic properties of the phosphors to be understood, including the direct band gap and the importance of empty rare-earth d states in the conduction band. We also explore cationic substitutions for $LaSr_2AlO_5:Ce^{3+}$ in an attempt to understand the influence of structural modifications on optical properties such as emission energy, quantum yield, and color rendering index R_a. Specifically, we have studied three different types of isovalent substitutions in $LaSr_2AlO_5:Ce^{3+}$: (i) for trivalent La, by the smaller trivalent rare-earths, Gd and Tb, in compositions of the type $La_{0.975-x}Ln_xCe_{0.025}Sr_2AlO_5$ (Ln = Gd, Tb); (ii) for divalent Sr, by the smaller divalent Ca, as well as by the larger divalent Ba, in compositions of the type $La_{0.975}Ce_{0.025}Sr_{2y}AE_{2-2y}AlO_5$ (AE = Ca, Ba); and (iii) for trivalent Al, by the smaller trivalent B, as well as by the larger trivalent Ga, in compositions of the type $La_{0.975}Ce_{0.025}Sr_2Al_{1-z}T_zO_5$ (T = B, Ga). Table 1 lists the ionic radii of the elements employed in the above sample preparations. We maintain 2.5 at % level of Ce^{3+} throughout, as it was found to yield the most efficient emission in the series $La_{1-x}Ce_xSr_2AlO_5$.[13] For all the compositions prepared, Rietveld analyses and photoluminescence measurements were performed for careful investigations of the composition-dependent variations of Ce−O bond distances and the emission properties. Finally, we describe the electroluminescence properties of some white light devices that make use of phosphor formulations developed in this work.

Table 2. List of Sample Compositions and Preparation Temperatures

sample	composition	T (°C)
Gd-0.1	$La_{0.875}Ce_{0.025}Gd_{0.1}Sr_2AlO_5$	1500
Gd-0.5	$La_{0.475}Ce_{0.025}Gd_{0.5}Sr_2AlO_5$	1500
Gd-1.0	$Gd_{0.975}Ce_{0.025}Sr_2AlO_5$	1500
Tb-0.1	$La_{0.875}Ce_{0.025}Tb_{0.1}Sr_2AlO_5$	1500
Tb-0.5	$La_{0.475}Ce_{0.025}Tb_{0.5}Sr_2AlO_5$	1500
Tb-1.0	$Tb_{0.975}Ce_{0.025}Sr_2AlO_5$	1500
Ca-0.1	$La_{0.975}Ce_{0.025}Sr_{1.8}Ca_{0.2}AlO_5$	1400
Ba-0.1	$La_{0.975}Ce_{0.025}Sr_{1.8}Ba_{0.2}AlO_5$	1400
Ba-0.5	$La_{0.975}Ce_{0.025}SrBaAlO_5$	1400
Ba-1.0	$La_{0.975}Ce_{0.025}Ba_2AlO_5$	1400
B-0.1	$La_{0.975}Ce_{0.025}Sr_2Al_{0.9}B_{0.1}O_5$	1400
Ga-0.1	$La_{0.975}Ce_{0.025}Sr_2Al_{0.9}Ga_{0.1}O_5$	1400
Ga-0.5	$La_{0.975}Ce_{0.025}Sr_2Al_{0.5}Ga_{0.5}O_5$	1400
Ga-1.0	$La_{0.975}Ce_{0.025}Sr_2GaO_5$	1400

Experimental Section

Powder samples of $La_{0.975-x}Ln_xCe_{0.025}Sr_2AlO_5$ (Ln = Gd, Tb), $La_{0.975}Ce_{0.025}Sr_{2-2y}AE_{2y}AlO_5$ (AE = Ca, Ba), and $La_{0.975}Ce_{0.025}Sr_2Al_{1-z}T_zO_5$ (T = B, Ga) were prepared by solid-state reactions using La_2O_3 (Aldrich, 99.9%), Gd_2O_3 (Aldrich, 99.9%), Tb_4O_7 (Aldrich, 99.9%), $SrCO_3$ (Aldrich, 99.995%), $BaCO_3$ (Alfa, 99.99%), $CaCO_3$ (Alfa, 99.99%), Al_2O_3 (Aldrich, 99.9%), H_3BO_3 (Aldrich, 99.9%), Ga_2O_3 (Aldrich, 99.9%), and CeO_2 (Aldrich, 99.9%). The powder reagents were quantitatively mixed using an agate mortar and pestle for 1 h and subsequently heated in the temperature range of 1400−1500 °C (see Table 2) in a reducing atmosphere of H_2/N_2 (5%/95%) for 4 h.

Room-temperature photoluminescence (PL) spectra were measured on a Perkin-Elmer LS55 luminescence spectrophotometer scanning the wavelength range of 300 to 760 nm. Diffuse reflectance absorption spectra were recorded using a Shimadzu UV-3600 spectrophotometer equipped with an ISR-3100 integrating sphere, in the wavelength range of 200−600 nm. For the calibration of diffuse-reflectance, $BaSO_4$ was used as a reference. The optical band gap was estimated by extrapolating the linear part of the absorption edge to zero-absorbance level.

Powder X-ray diffraction (XRD) data were obtained using Cu $K\alpha$ radiation (Philips X′Pert) over the angular range $20° \leq 2\theta \leq 100°$ with a step size of 0.016°. Crystal structure refinements were performed by Rietveld method using the General Structure Analysis System (GSAS) software suite.[18]

Prototype LED devices were fabricated by applying an intimate mixture of two or three different phosphor compositions and transparent silicone resin on commercially available InGaN LEDs (λ_{max} = 450, 460 nm) to an active area of 470 × 250 μm^2. Luminescence spectra were acquired with diodes subjected to forward biases of varying constant currents, with the light output collected and measured using an integrating sphere.

Computational Details

Linear muffin tin orbital (LMTO) calculations[19,20] were performed to investigate the electronic band structure of the host compound, $LaSr_2AlO_5$. Scalar-relativistic Kohn−Sham

(14) Park, J. K.; Choi, K. J.; Kim, K. N.; Kim, C. H. *Appl. Phys. Lett.* **2005**, *87*, 031108.
(15) Blasse G.; Grabmaier, B. C. Luminescent Materials; Springer: Berlin, 1994.
(16) Shinoya, S.; Yen, W. M. Phosphor Handbook; CRC Press: Boca Raton, FL, 1998.
(17) Drofenik, M.; Golic, L. *Acta Crystallogr., Sect. B* **1979**, *35*, 1059.
(18) Larson, A. C.; Von Dreele, R. B. General Structure Analysis System (GSAS); Los Alamos National Laboratory Report LAUR 86-748; Los Alamos National Laboratory: Los Alamos, NM, 1994.
(19) Andersen, O. K. *Phys. Rev. B* **1975**, *12*, 3060.
(20) Jepsen, O.; Andersen, O. K. *Z. Phys. B* **1995**, *97*, 35.
(21) von Barth, U.; Hedin, L. *J. Phys. C.* **1972**, *5*, 1629.

equations were solved using the local-density approximation (LDA) of density functional theory.[21] All relativistic effects were taken into account except for spin−orbit coupling. The crystal structure input for the calculation was obtained from the experimental (Rietveld) crystal structure of $LaSr_2AlO_5$ by constructing an ordered supercell in the *Fmmm* space group, with the cell parameters $a = c_{tet}$ and $b = c = \sqrt{2}a_{tet}$. The subscript "tet" here refers to the *I*4/*mcm* structure of $LaSr_2AlO_5$. The supercell had La and Sr ordered in a checkerboard on the 8*h* sites of the original crystal structure. The calculations were performed on a grid of 95 irreducible *k* points within the primitive edge of the Brillouin zone. The Stuttgart TB-LMTO-ASA program (version 47C) was used for the computation.[22]

Results

Structural and Optical Properties of the Basis Composition $La_{0.975}Ce_{0.025}Sr_2AlO_5$. In the present study, the Ce^{3+} content in all the samples was fixed at 2.5% of the total rare earth, regardless of the substitution sites in the parent structure. We therefore begin with the description of structural and optical properties of $La_{0.975}Ce_{0.025}Sr_2AlO_5$, which represents the basis composition of all substitutional derivatives. (Hereafter, the acronym LSA:Ce^{3+} refers to the specific composition $La_{0.975}Ce_{0.025}Sr_2AlO_5$.) For the structure refinement of LSA:Ce^{3+}, the starting model was the single-crystal structure of $EuSr_2AlO_5$. Because the ionic radii of 8-coordinate La^{3+} (1.160 Å) and Eu^{3+} (1.066 Å) differ only moderately,[24] it is reasonably assumed that the two compounds have a common crystal structure. Structurally, $EuSr_2AlO_5$ belongs to the Cs_3CoCl_5-family (tetragonal, space group *I*4/*mcm*), and is also closely related with the $Ba_3M^{4+}O_5$-type compounds (tetragonal, space group *P*4/*ncc*).[23] Thus, first of all, we carefully examined the extinction conditions of observed XRD pattern and confirmed that LSA:Ce^{3+} crystallizes in the space group *I*4/*mcm*, not in *P*4/*ncc*. In the unit cell ($Z = 4$) of LSA:Ce^{3+}, we presume that Ce and La atoms occupy only the 8*h* positions without any site-mixing. Half the 8*h* sites are expected to be filled by Ce and La atoms, and the other half by Sr atoms (Sr1). The cell also contains the 4*a* site fully occupied by Sr atoms (Sr2), and the 4*b* site occupied by Al atoms. Oxygen atoms are distributed over the 4*c* site and the 16*l* site, denoted as O1 and O2, respectively. In the refinement procedure, the occupancy parameters of all the constituent atoms were fixed to the nominal stoichiometry, and the temperature factors for La, Ce, and Sr atoms on 8*h* position were constrained to be equal.

Figure 1 shows the results of Rietveld profile refinement for LSA:Ce^{3+}, obtained with goodness of fit parameters $R_{wp} = 3.63\%$ and $\chi^2 = 1.295$. Structural parameters of LSA:Ce^{3+} and selected bond lengths/angles are listed in Table 3 and Table 4, respectively. Compared with $EuSr_2AlO_5$, LSA:Ce^{3+} has an expanded

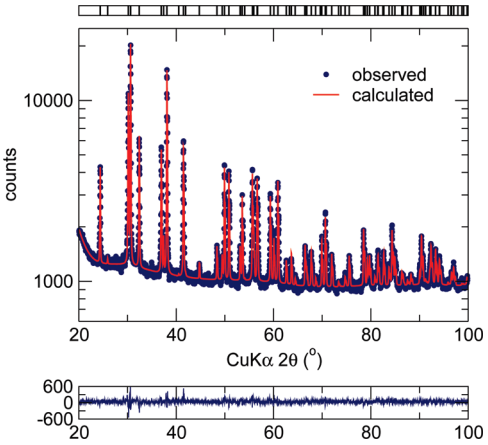

Figure 1. Rietveld refinement of powder XRD profile of LSA:Ce^{3+}. Observed (circles), calculated (red line), and difference profiles are displayed along with expected reflection positions.

Table 3. Structural Parameters for $La_{0.975}Ce_{0.025}Sr_2AlO_5$ as Determined by Rietveld Refinement of Powder XRD Data at Room Temperature[a]

atom	site	*x*	*y*	*z*	*g*	U_{iso} (Å^2)[b]
La	8*h*	0.3198(9)	0.1802(9)	0	0.4875	0.0085(1)
Ce	8*h*	0.3198(9)	0.1802(9)	0	0.0125	0.0085(1)
Sr1	8*h*	0.3198(9)	0.1802(9)	0	0.5	0.0085(1)
Sr2	4*a*	0	0	1/4	1.0	0.0081(1)
Al	4*b*	1/2	0	1/4	1.0	0.0042(1)
O1	4*c*	0	0	0	1.0	0.0230(1)
O2	16*l*	0.1346(6)	0.3654(6)	0.1485(4)	1.0	0.0074(1)

[a] Space group: *I*4/*mcm* (No. 140), $Z = 4$, $V = 524.44(4)$ Å^3. $a = b = 6.8856(2)$ Å, $c = 11.0613(1)$ Å. [b] Constraints on isotropic thermal factors: U_{iso} (La) = U_{iso} (Ce) = U_{iso} (Sr1).

Table 4. Selected Bond Distances and Angles in $La_{0.975}Ce_{0.025}Sr_2AlO_5$

bond distance (Å)		angle (deg)	
La/Ce−O1	(2 ×) 2.527(1)	O2−Al−O2	(4 ×) 115.05(1)
La/Ce−O2	(2 ×) 2.440(5)		(2 ×) 98.81(3)
	(4 ×) 2.738(4)		
Al−O2	(4 ×) 1.726(5)		

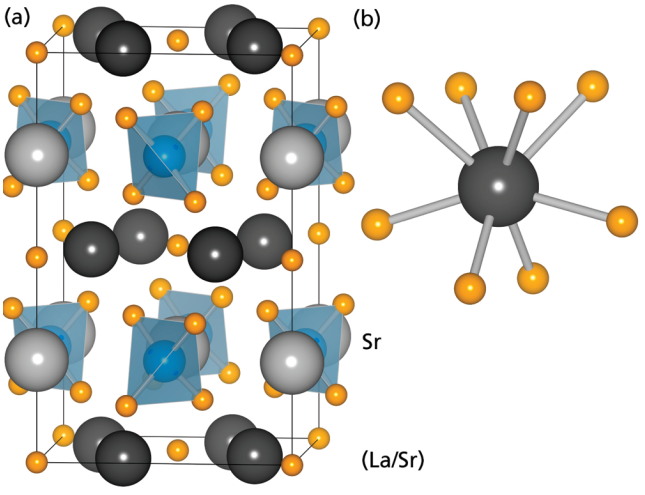

Figure 2. (a) Unit-cell representation of LSA:Ce^{3+} and (b) coordination geometry of CeO_8 polyhedron therein. Light gray, blue, and orange spheres represent Sr, Al, and O atoms, respectively. Dark gray spheres are populated by La, Sr, and Ce atoms.

(22) Jepsen, O.; Andersen, O. K. The Stuttgart TB-LMTO-ASA Program, version 47; MPI fr Festkorperforschung: Stuttgart, Germany, 2000.
(23) Dent, L. S.; Glasser, F. P. *Acta Crystallogr.* **1965**, *18*, 453.
(24) Shannon, R. D. *Acta Crystallogr., Sect. A* **1976**, *32*, 751.

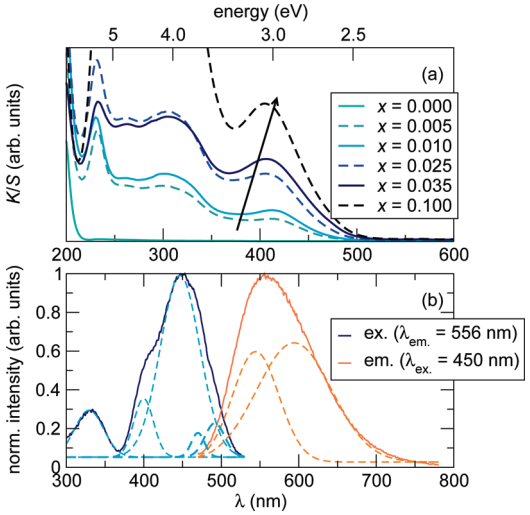

Figure 3. (a) Diffuse-reflectance spectra for $La_{1-x}Ce_xSr_2AlO_5$ and (b) excitation and emission spectra of LSA:Ce^{3+}. Peak deconvolution of excitation and emission bands are indicated as dotted lines.

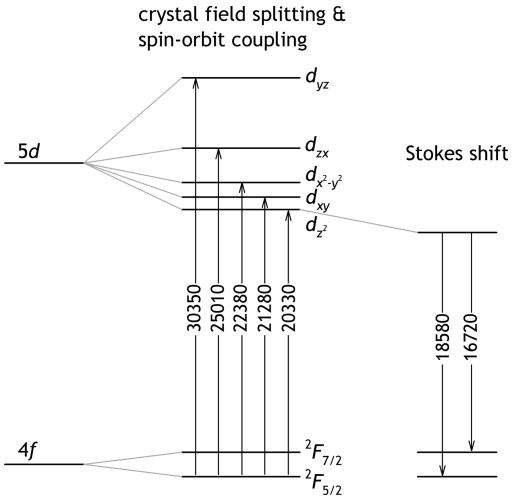

Figure 4. Schematic energy structure of Ce 4f and 5d levels in LSA:Ce^{3+}. Numbers shown over the arrows denote the corresponding transition energies in cm^{-1}.

tetragonal cell, in agreement with the ionic radius of La^{3+} being larger than that of Eu^{3+}.

As presented in Figure 2, the LSA:Ce^{3+} lattice is composed of (La,Ce)SrO^{3+} layers ($z_{La} = z_{Sr} = 0$ or 1/2) alternating with $SrAlO_4^{3-}$ layers ($z_{Sr} = z_{Al} = 1/4$ or 3/4) along the *c*-axis. The CeO_8 polyhedron consists of two O1 atoms on the 4*c* site and six O2 atoms on the 16*l* site, where the latter are shared by four AlO_4 tetrahedra on the adjacent layers. The polyhedral geometry around Ce atom can be described as a distorted square antiprism, in which the two O1 atoms are displaced away from each other, while residing on the mirror plane. For such a coordination environment, the five Ce 5d orbitals are split into five different levels, in the increasing order of energy d_{z^2}, d_{xy}, $d_{x^2-y^2}$, d_{zx}, and d_{yz}. Because emission in the LSA:Ce^{3+} phosphor occurs mostly from the lowest-lying 5d level of Ce, $5d_{z^2}$ in this case, any deformation of the CeO_8 geometry can alter the crystal field splitting pattern and result in a shift of emission band positions and widths.[34] In simple examples of isotropic volume changes, contraction of CeO_8 polyhedra will strengthen the crystal field around Ce^{3+} and increase the emission wavelength, whereas the expansion will result in the opposite effect.

Figure 3a shows the diffuse reflectance absorption spectra for $La_{1-x}Ce_xSr_2AlO_5$ ($x = 0$ to 0.1) samples, where the Kubelka−Munk absorption coefficient (K/S) was calculated from the measured reflectance (R) following the relation[25,26]

$$\frac{K}{S} = \frac{(1-R)^2}{2R} \qquad (1)$$

The undoped phase $LaSr_2AlO_5$ (LSA), exhibits no absorption in the wavelength range below 380 nm and accordingly is white in color. The band gap energy (E_g) of LSA is estimated to be ~5.9 eV. However, Ce substitution causes an immediate change in the optical behavior of LSA, as indicated by the appearance of absorption peak at $\lambda = 420$ nm. Already at $x = 0.005$, the $La_{1-x}Ce_xSr_2AlO_5$ sample turns yellow in color, owing to the 4f → 5d absorption transition at the Ce^{3+} center. The increase of Ce^{3+} concentration accompanies enhancement of the absorption, and also a gradual red shift of the absorption edge. It is clear therefore that the dopant Ce^{3+} creates localized energy levels within the electronic structure of the LSA host, and provide absorption pathways for visible light.

To probe the energy structure of the Ce 5d and 4f levels in LSA:Ce^{3+}, the excitation ($\lambda_{em} = 556$ nm) and emission ($\lambda_{ex} = 450$ nm) spectra were analyzed by the peak deconvolution of Gaussian components. The normalized emission and excitation spectra of LSA:Ce^{3+} are shown in Figure 3b. The asymmetric emission band is fitted as the sum of two components, accounting for the transitions from the lowest-lying excited state $5d_{z^2}$ to the $^2F_{5/2}$ and $^2F_{7/2}$ ground states. Although the 5d orbital energies of Ce are split by the crystal field, the $4f^1$ configuration has two states split by spin−orbit coupling. The magnitude of the spin−orbit coupling is determined to be 1860 cm^{-1} from the separation between the fitted peak positions of 538 and 598 nm. On the other hand the excitation spectrum comprises five peak components, corresponding to excitations from $^2F_{5/2}$ state to five different levels of 5d orbitals. Excitation from the $^2F_{7/2}$ state can be ignored, because the spin−orbit splitting (1860 cm^{-1} = 231 meV) is far larger than k_BT (26 meV) at 300 K. On the basis of the peak deconvolution result and the transition paths described above, an energy level scheme for Ce^{3+} in LSA:Ce^{3+} is proposed as illustrated in Figure 4.

Previously, we observed that quenching of emission intensity occurs when x exceeds 0.025 in $La_{1-x}Ce_xSr_2AlO_5$, namely the critical concentration x_c is 0.025.[13] The critical distance for energy transfer (R_c) in $La_{1-x}Ce_xSr_2AlO_5$ can be calculated from the structural parameters

(25) Kubelka, P.; Munk, F. *Z. Tech. Phys.* **1931**, *12*, 593.
(26) Kim, Y.-I.; Page, K.; Limarga, A. M.; Clarke, D. R.; Seshadri, R. *Phys. Rev. B* **2007**, *76*, 115204.
(27) Blasse, G. *Philips Res. Rep.* **1969**, *24*, 131.

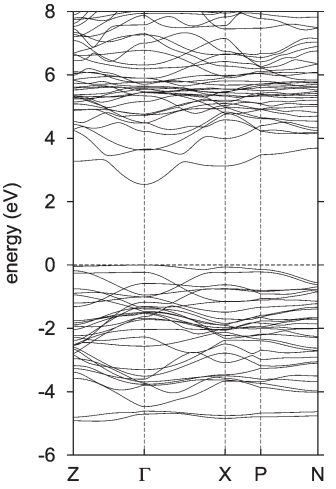

Figure 5. LMTO-ASA energy bands of an $LaSr_2AlO_5$ supercell with La and Sr ordered in a checkerboard manner on the original 8*h* sites of the tetragonal crystal structure.

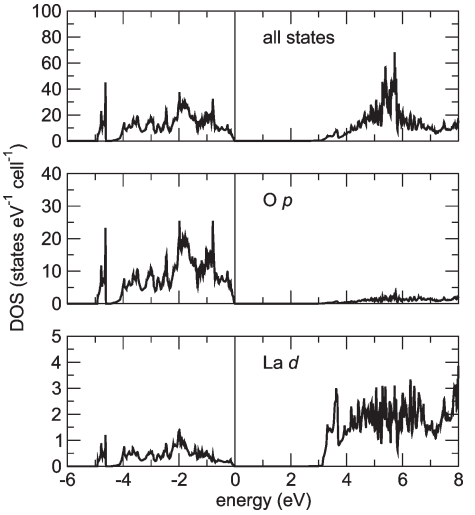

Figure 6. Total and projected LMTO-ASA densities of state for $LaSr_2AlO_5$.

such as unit-cell volume (V) and number of total Ce^{3+} sites per unit cell (N), together with x_c.[27]

$$R_c \approx 2\left(\frac{3V}{4\pi x_c N}\right)^{1/3} \quad (2)$$

Here R_c corresponds to the mean separation between the nearest Ce^{3+} ions at the critical concentration. Using $V = 524.4$ Å^3, $N = 4$, and $x_c = 0.025$, the critical transfer distance of Ce^{3+} in $La_{1-x}Ce_xSr_2AlO_5$ is determined to be ~21 Å, which is close to the value of ~19 Å obtained using Dexter's formula.[13,28] To assess the efficiency of luminescence, we measured quantum efficiency (QE) using excitation source of 457 nm from an argon laser, using a setup described by Greenham et al.[29] The QE from LSA:Ce^{3+} was obtained to be 42% at room temperature, as compared with 75% obtained from a commercial reference YAG:Ce^{3+} sample. We note that the emission band of LSA:Ce^{3+} is somewhat wider than that of YAG:Ce^{3+}, with the full width at half-maximum (fwhm) values of 116 and 104 nm, respectively. This implies that LSA:Ce^{3+} may provide an improved color rendering when incorporated in LED lamps. From the lowest excitation energy and the higher emission energy, the Stokes shift in LSA:Ce^{3+} is estimated to be 1750 cm^{-1}, and the 5d crystal field splitting to be 10020 cm^{-1}. For comparison, YAG:Ce^{3+} is reported to have a Stokes shift of 3800 cm^{-1} and a crystal field splitting of 28300 cm^{-1}.[30]

Band Structure and Densities of State. We considered it of some interest to examine the electronic structure of the host compound LSA using density functional theory (DFT). DFT electronic structure is rarely employed for understanding and designing of new phosphor hosts. The reasons for this are many and include the inability of DFT in its usual implementations to accurately describe f orbitals, and unoccupied states, and the general difficulty of carrying out electronic structure calculations on systems with small substitution; the phosphor system being closer to a defect state than an actual crystalline material. We nevertheless present results here in the hope that they encourage the further use of DFT in predicting trends in crystal fields of various host compounds. The band structure of the ordered supercell of LSA is displayed in Figure 5. LSA is seen to be a direct band gap material within DFT-LDA near 2.5 eV. This is much smaller than the experimental value measured here. This underestimation is somewhat typical of calculations on crystal structures with very low band dispersion. The calculated band gap is rather sensitive to the nature of the ordering of La and Sr in the supercell. We determined that at least one alternative ordering (chains of La and Sr, rather than a checkerboard, in a supercell in space group *Ima*2) resulted in a calculated band gap that was even smaller, near 1.5 eV, presumably as a result of greater La−O−La dispersion along the chains. The use of a gradient approximation is seen to increase the band gap to about 3.0 eV.

Figure 6 displays the LMTO-ASA densities of states of the LSA supercell. The valence band is seen to comprise mostly O−p derived states, while the lowest part of the conduction band is mainly contributed from the La d states. The rest of the conduction band derives largely from empty spheres used in the calculation. This computation result suggests that LSA has a proper electronic structure for serving as a Ce^{3+} phosphor host. Although not explicit from the present calculation, it is reasonable to expect that a Ce^{3+} dopant would have the empty d states near the bottom of conduction band, and that the singly occupied f orbital be situated in the valence band. Because the band gap of LSA is not very wide, as judged by both the experimental measurement and the calculation, there is a high chance that the dopant's 4f−5d separation would fall in the visible light range. Analysis of the excitation spectrum for LSA:Ce^{3+} indicates that the

(28) Dexter, D. L. *J. Chem. Phys.* **1953**, *21*, 836.
(29) Greenham, N. C.; Samuel, I. D. W.; Hayes, G. R.; Phillips, R. T.; Kessener, Y. A. R. R.; Moratti, S. C.; Holmes, A. B.; Friend, R. H. *Chem. Phys. Lett.* **1995**, *241*, 89.
(30) Tomiki, T.; Akamine, H.; Gushiken, M.; Kinjoh, Y.; Miyazato, M.; Miyazato, T.; Toyokawa, N.; Hiraoka, M.; Hirata, N.; Ganaha, Y.; Futemma, T. *J. Phys. Soc. Jpn.* **1991**, *60*, 2437.

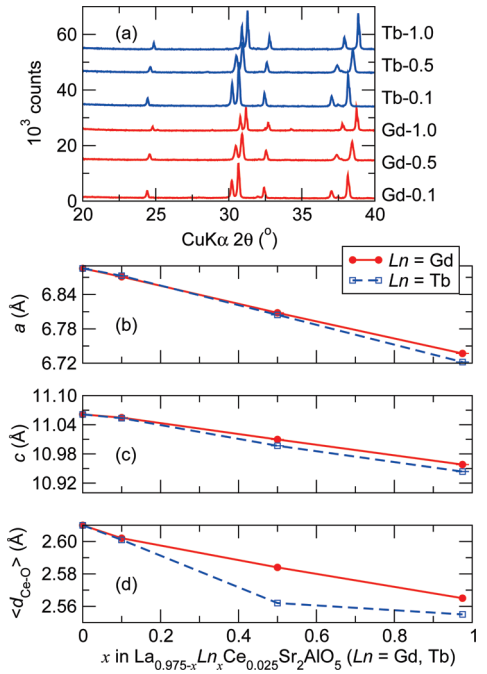

Figure 7. (a) Powder XRD patterns of $La_{0.975-x}Ln_xCe_{0.025}Sr_2AlO_5$ (*Ln* = Tb, Gd; x = 0.1, 0.5, and 0.975) and Rietveld refined results (b) lattice constant *a*, (c) lattice constant *c*, and (d) mean interatomic distance of Ce−O.

centroids of Ce 4f and 5d levels are separated by ~3.0 eV (23900 cm^{-1}), suitable for the absorption/emission of visible light. It is worth making a comparison with the canonical yellow phosphor YAG:Ce^{3+} that is distinct from LSA:Ce^{3+}. YAG has a wider band gap of 6.5 eV,[31] and accordingly the centroids of Ce 4f and 5d levels in YAG:Ce^{3+} are as distant as 4.3 eV (34500 cm^{-1}). However, YAG:Ce^{3+} provides a large crystal field splitting for the dopant Ce^{3+}, so that its lowest 5d level lies only 2.7 eV (21700 cm^{-1}) above the ground ^2F states. The difference in the crystal fields of YAG and LSA arises from the ion packing pattern in respective crystal types. In the compact garnet structure of YAG, the eight Y−O bonds have an average distance of 2.37 Å,[32] while the La−O bond distances in LSA are averaged to 2.61 Å. As described here, the activator ion's f−d separation, i.e., the excitation/emission characteristics of the phosphor, is determined by the electronic structure of the host as well as the coordination environments for the doping site. We suggest that the DFT studies can help sort out potential phosphor hosts by allowing rough estimations of the band gap width, and no less importantly by revealing the main component in the conduction band minimum.

$La_{0.975-x}Ln_xCe_{0.025}Sr_2AlO_5$ (*Ln* = Tb, Gd; x = 0.1, 0.5, and 0.975). Substitution of the basis composition LSA:Ce^{3+} was explored for each of the three cation types La, Sr, and Al. By employing isovalent substituents with varying sizes, we could alter the structural environment for Ce^{3+} ions and thereby the crystal field splitting of

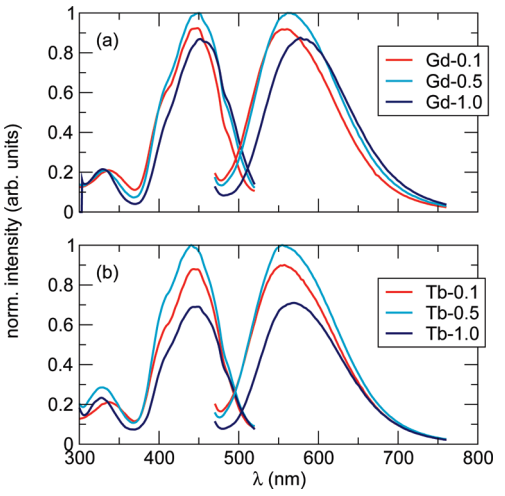

Figure 8. Normalized PL spectra: (a) excitation and (b) emission of $La_{0.975-x}Ln_xCe_{0.025}Sr_2AlO_5$ (*Ln* = Tb, Gd; x = 0.1, 0.5, and 0.975).

Table 5. Spectral Parameters for $La_{0.975-x}Ln_xCe_{0.025}Sr_2AlO_5$ (*Ln* = Tb, Gd; x = 0.1, 0.5, and 0.975), Peak Positions from Excitation (P_{ex}) and Emission (P_{em}), and Emission Width ($fwhm_{em}$)

sample	P_{ex}(nm)	P_{em} (nm)	$fwhm_{em}$ (nm)
LSA:Ce^{3+}	334/450	556	116
Gd-0.1	335/448	560	121.5
Gd-0.5	332/449	562	120.5
Gd-1.0	329/452	577	119
Tb-0.1	334/443	552	121
Tb-0.5	327/440	554	121.5
Tb-1.0	325/449	569	119

Ce 5d levels. First, the substitution of La^{3+} by Gd^{3+} and Tb^{3+} was studied, both ions being known to be compatible with the phosphor host lattice.[6,7,33] It has been recently reported that the substitution of Tb^{3+} for Y^{3+} in YAG:Ce^{3+} gives rise to better efficiency and color rendering properties of the LED device.[6,7]

Figure 7a shows the XRD patterns of $La_{0.975-x}Ln_xCe_{0.025}Sr_2AlO_5$ (*Ln* = Tb, Gd; x = 0.1, 0.5, and 0.975). In accordance with the ionic size variation, Tb- or Gd-substitution for La results in the shift of diffraction peaks to higher angle region. However there was no evidence of a structural transition with increasing substitution in either case. Therefore the Rietveld refinements were carried out assuming that the *Ln* atoms substitute only for La, with their occupancies equal to the respective nominal amounts. In all six cases, the structure refinements converged with final R_{wp} values of 3−4%. The lattice parameters for $La_{0.975-x}Ln_xCe_{0.025}Sr_2AlO_5$ phases as determined from Rietveld profile analysis are plotted in panels b and c in Figure 7. With increasing amounts of Tb or Gd, the tetragonal cell parameters gradually decrease, indicating that the solid solutions $La_{0.975-x}Ln_xCe_{0.025}Sr_2AlO_5$ (*Ln* = Tb, Gd) occur in the entire x range of 0−0.975, while retaining the same crystal structure.

We note that the above lanthanide substitution causes only subtle changes of the tetragonal aspect ratio and also

(31) Slack, G. A.; Oliver, D. W.; Chrenko, R. M.; Roberts, S. *Phys. Rev.* **1969**, *177*, 1308.
(32) Nakatsuka, A.; Yoshiasa, A.; Yamanaka, T. *Acta Crystallogr., Sect. B* **1999**, *55*, 266.
(33) Tien, T. Y.; Gibbons, E. F.; DeLosh, R. G.; Zacmanidis, P. J.; Smith, D. E.; Stadler, H. L. *J. Electrochem. Soc.* **1973**, *120*, 278.

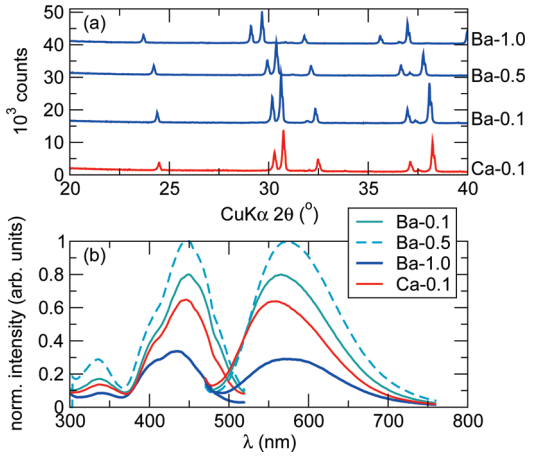

Figure 9. (a) Powder XRD patterns and (b) normalized excitation and emission spectra of $La_{0.975-x}Ln_xCe_{0.025}Sr_{2-2y}AE_{2y}AlO_5$ (AE = Ca, Ba; y = 0.1, 0.5, and 1.0).

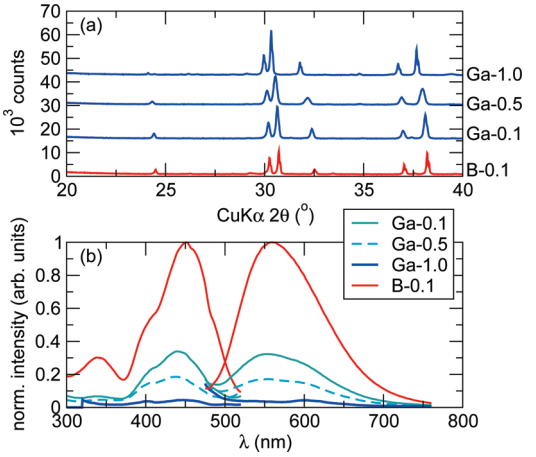

Figure 10. (a) Powder XRD patterns and (b) normalized excitation and emission spectra of $La_{0.975}Ce_{0.025}Sr_2Al_{1-z}T_zO_5$ (T = B, Ga; z = 0.1, 0.5, and 1.0).

of the bond angles within the internal CeO_8 polyhedra. Given this, it can be assumed that the crystal field around Ce^{3+} is dictated mostly by the volume of the CeO_8 polyhedra, in other words, the mean Ce−O distance. As represented in Figure 7d, the substitutions of Tb or Gd for La result in the contraction of Ce−O bonds, which is in turn expected to decrease the emission band energy. Indeed the emission from $La_{0.975-x}Gd_xCe_{0.025}Sr_2AlO_5$ samples show a clear red shift with x, consistent with the changes of Ce−O distances [Figure 8a and Table 5]. From LSA:Ce^{3+} to Gd-1.0, the peak of the emission band shifts by more than 20 nm (from 556 to 577 nm). On the other hand, the emission band shifts in $La_{0.975-x}Tb_xCe_{0.025}Sr_2AlO_5$ samples are somewhat smaller than projected: For x = 0.1, 0.5, and 0.975, the peak positions are located at 552, 554, and 569 nm, respectively. It implies that the emission energy in Tb-rich lattice is governed not simply by the crystal field but also by the covalency factor. It is regarded that the Tb-substitution for La atoms increase the lattice ionicity, which contribute to widening the Ce 4f−5d separation. This point is discussed more extensively in a later section.

$La_{0.975}Ce_{0.025}Sr_{2-2y}AE_{2y}AlO_5$ (AE = Ca, Ba, y = 0.1, 0.5, and 1.0). Next we have investigated the effect of alkaline-earth substitution in LSA:Ce^{3+}, by replacing Sr atoms by Ba or Ca atoms. In the Ba case, single-phase products were formed from all the compositions of y = 0.1, 0.5, and 1.0 as demonstrated by the XRD patterns shown in Figure 9a. However complete Ca substitution could not be accomplished, and single-phase samples were obtained only at y = 0.1. In the preparative attempts using calcium contents of y = 0.5 and 1.0, the Ruddlesden−Popper compound La(Ca,Sr)AlO_4 was found to be a robust competing phase.

Strontium in the parent LSA:Ce^{3+} structure has, unlike La or Al, two crystallographically distinct sites, 8*h* (Sr1) and 4*a* (Sr2). Thus depending on the preferential occupation of AE atom on either of 8*h* or 4*a* sites, the substitution compounds $La_{0.975}Ce_{0.025}Sr_{2-2y}AE_{2y}AlO_5$ can have different structural and optical properties. Note that Sr1 atoms share a common site with rare-earth atoms, whereas Sr2 atoms are proximately located to the AlO_4 units. Therefore in the structure refinements of $La_{0.975}Ce_{0.025}Sr_{2-2y}AE_{2y}AlO_5$, AE atoms were allowed to occupy both 8*h* and 4*a* sites. For the four single phase samples of $La_{0.975}Ce_{0.025}Sr_{2-2y}AE_{2y}AlO_5$, Rietveld refinements have been performed, where the final R_{wp} values were 6.4−6.7%. Rather high R_{wp} values here, compared with those for lanthanide substitution compounds, are possibly due to the greater lattice strain associated with the alkaline-earth substitution. Although the Ln-substitutions suffer only mild size mismatches among $Ln^{3+}/La^{3+}/Sr^{2+}$ (Ln = Tb, Gd) on the 8*h* site, the AE-substitutions will involve more complicated disorders arising from the mixed occupations of AE^{2+}/Sr^{2+} on the 4*a* site and $AE^{2+}/Sr^{2+}/La^{3+}$ (AE = Ca, Ba) on the 8*h* site. Obviously, the lattice formed of the latter configuration will contain irregular local structures largely departed from the average structure. In such cases, the diffraction peak profiles become broadened in a way that is difficult to model. As given in Table 1, the size of the Ba^{2+} ion is better suited to the 4*a* site (CN = 10) than to the 8*h* one (CN = 8). Not surprisingly, the Rietveld analyses of the Ba-0.1 and Ba-0.5 phases revealed that Ba atom has a high preference for the 4*a* (Sr2) site. On the other hand, the Ca atom in the Ca-0.1 favors the 8*h* site (CN = 8) due to the similarity of ionic radii between Ca^{2+} and La^{3+}. The mean Ce−O distance in the Ca-0.1 phase is slightly shorter than that of LSA:Ce^{3+}, because the Ca-substitution occurs mostly on the 8*h* site. However, the Ba substitution generally increases the Ce−O distance, from 2.59 Å in Ba-0.1 to 2.67 Å in Ba-1.0. These results are consistent with the relative sizes of Ca^{2+}, Ba^{2+}, and Sr^{2+} ions (Table 1).

Table 6. Spectral Parameters for $La_{0.975}Ce_{0.025}Sr_{2-2y}AE_{2y}AlO_5$ (AE = Ca, Ba; y = 0.1, 0.5, and 1.0)

sample	P_{ex} (nm)	P_{em} (nm)	fwhm$_{em}$ (nm)
Ba-0.1	337/449	565	120.5
Ba-0.5	335/449	573	122.5
Ba-1.0	340/435	577	133
Ca-0.1	336/446	559	122

Table 7. Spectral Parameters for $La_{0.975}Ce_{0.025}Sr_2Al_{1-z}T_zO_5$ (T = B, Ga; z = 0.1 and 0.5)

sample	P_{ex} (nm)	P_{em} (nm)	fwhm$_{em}$ (nm)
Ga-0.1	339/439	551	130
Ga-0.5	338/438	547	142
B-0.1	338/451	558	120

Figure 9b presents the PL spectra of the Ba-0.1, Ba-0.5, Ba-1.0, and Ca-0.1 samples. Although the mean Ce−O distance increases with the progress of Ba-substitution, the respective emission peak positions display red shifts, from 565 nm for Ba-0.1 to 577 nm for Ba-1.0 (see Table 6). This can be attributed to the dominance of covalency effects over the crystal field effect. On the other hand, the peak position of Ca-0.1 phase was located at 559 nm, which is in accord with the crystal field strength expected for a relatively short mean Ce−O distance 2.59 Å. The emission intensities of Ba-0.1 and Ba-0.5 phases are comparable to or even enhanced from that of unsubstituted LSA:Ce^{3+}, but the emission drastically decreases in the Ba-1.0 phase. Taking into account the Rietveld refinement results, we propose that Ba at the 4*a* site improves the luminescence behavior, while the Ba at the 8*h* site has an adverse impact. Further experimental studies are under way to clarify the structural details and their correlation with the optical properties of $La_{0.975}Ce_{0.025}Sr_{2-2y}Ba_{2y}AlO_5$.

$La_{0.975}Ce_{0.025}Sr_2Al_{1-z}T_zO_5$ (T = B, Ga, z = 0.1, 0.5, and 1.0). For exploring the substitution of Al atom in LSA:Ce^{3+}, two congenor elements B and Ga were employed as substituent. As illustrated in Figure 2, AlO_4 tetrahedra serve as the key structural component in LSA:Ce^{3+}. Moreover the optically active CeO_8 polyhedron shares two edges and two corners with the nearby AlO_4 tetrahedra. It is therefore expected that the substitution of Al will critically affect the luminescence properties of LSA:Ce^{3+}, as well as its phase stability. As judged from the XRD profiles in Figure 10a, Ga-substitutions produce near-single phase structures in all cases of z = 0.1, 0.5, and 1.0. The samples of T = Ga contained small amounts of LaSr(Al,Ga)O_4 as secondary phases, but with the respective fractions constant regardless of z. On the other hand the B-substitution resulted in a single phase structure only for z = 0.1, apparently due to the marked size difference between B^{3+} and Al^{3+} ions (Table 1). Interestingly, the B-0.1 sample was almost free of the competing Ruddlesden−Popper phase, $LaSrAlO_4$.

As for the phosphor efficiency, substitution of Ga for Al atom leads to abrupt degradation of the overall emission performances. Figure 10b and Table 7 show that the emission band becomes gradually weaker and broader upon the Ga-substitution. However the B-substitution for Al caused only a slight change of the luminescence property. We believe that structural factors are primarily involved in the depressed emission property of Ga-substituted samples. The compositional inhomogeneity between Ga/Al can disturb the lattice perfection near the z = 1/4 and 3/4 layers, as is observed from the broadening of XRD (00*l*) peaks. For instance, the (004) peaks near 32° have the fwhm values of 0.10, 0.15, 0.26, and 0.12°, for LSA:Ce^{3+}, Ga-0.1, Ga-0.5, and Ga-1.0 phases, respectively. Although the two end members of solid solution, LSA:Ce^{3+} and Ga-1.0, exhibit fairly narrow (004) peak widths, the other two with Al/Ga mixing show clear indication of peak broadening. We infer that the z-positions of O_2 atom groups or the (Al,Ga) atom groups are somewhat scattered in Ga-0.1 and Ga-0.5 samples, and such disorder grows in parallel with the mixing entropy. The irregularity in the crystal lattice will provide abundant defect centers to facilitate nonradiative decay.[15,16,36,37] The above disorder effect is most pronounced for the Al/Ga solid solution, which we attribute to the fact that the AlO_4 tetrahedra are intrinsically rigid structure-directing moieties. Although mixing disorder should be absent in the Ga-1.0 phase, we observe that the luminescence vanishes at full Ga substitution. We speculate that the incorporation of Ga deteriorates the ability of LSA to serve as a phosphor host, possibly through quenching by the heavier Ga. Similar behavior has been previously reported for the $Y_3Al_{5-x}Ga_xO_{12}$:Ce^{3+} garnet phosphors, that the increase of Ga content lowers the emission efficiency, with the phase of x = 5 being nonfluorescent.[38]

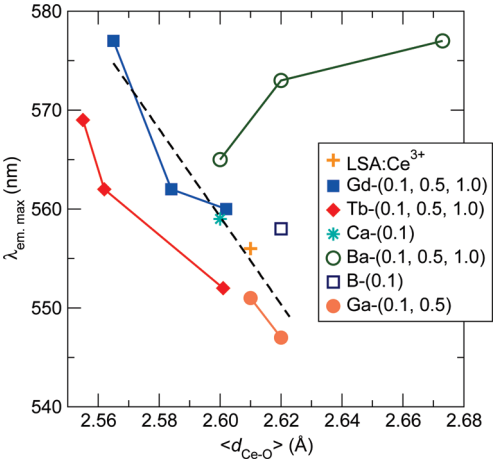

Figure 11. Mean Ce−O distances and emission peak positions of the LSA:Ce^{3+}-based phosphors. Broken line is a guide to the eyes.

Tuning Optical Properties and Phase Stability of LSA-Based Phosphors. Figure 11 presents a summary of the emission behaviors of LSA-based phosphors studied in this work. To enable comparisons among different substitution derivatives, the mean Ce−O distance ($\langle d_{Ce-O}\rangle$) and the peak energy of emission band were chosen to represent the structural and optical characteristics, respectively. As noted here, $\langle d_{Ce-O}\rangle$ can be a proper measure of the volume of the CeO_8 polyhedra and the magnitude of the relevant crystal field splitting. On the

(34) Palilla, F. C.; Levine, A. K.; Tomkus, M. R. *J. Electrochem. Soc.* **1968**, *115*, 642.
(35) Rack, P. D.; Holloway, P. H. *Mater. Sci. Eng., R* **1998**, *21*, 171.
(36) Chen, L.-T.; Hwang, C.-S.; Chen, I.-G.; Chang, S.-J. *J. Alloys Compd.* **2006**, *426*, 395.
(37) Wells, J.-P. R.; Yamaga, M.; Han, T. P. J.; Mosses, R. W. *Radiat. Eff. Defects Solids* **1999**, *149*, 341.
(38) Blasse, G.; Bril, A. *J. Chem. Phys.* **1967**, *47*, 5139.

basis of the point charge model, the d-orbital splitting of a metal center is given as[35]

$$Dq = \frac{Z^* e^2 r^4}{6R^5} \quad (3)$$

where Dq corresponds to the energy level separation, Z^* is the valence of the anion ligand, e is electron charge, r is the radius of frontier d wave function, and R is the distance between the metal center and ligand. From $Dq \propto R^{-5}$, even a small change in $\langle d_{Ce-O} \rangle$ should significantly alter the observed emission energies. Other factors being equal, when the metal−ligand distance decreases, the repulsive electrostatic interactions increase, and so does crystal field splitting. As a net effect, the lowest-lying Ce 5d level moves downward in energy, resulting in the red shift of emission wavelengths. The lattice ionicity of the host is another important variable that influences on the emission energies. In the lattice environment with increased bond covalency, the 4f and 5d levels of Ce^{3+} become less well separated, and the 5d → 4f emission occurs at longer wavelengths.

As shown in Figure 11, the LSA-based phosphor compositions from six substitution sets feature a wide range of emission peak wavelength (545−577 nm) as resulting from the modulation of $\langle d_{Ce-O} \rangle$ between 2.55 and 2.67 Å. The majority of the thirteen data points conform to the prediction that the emission will shift to longer wavelength when the Ce−O pairs get closer, but we also find some large departures from the ideal correlation. Although the Gd-substituted phases are well-behaved, the Tb-substituted ones show emission peaks at much shorter wavelengths than expected. This observation suggests that the incorporation of Tb modifies the bonding character of LSA lattice quite effectively in a way to decrease the covalency. For Tb-0.1 and Tb-0.5 phases, the ionicity contribution appears to be the prevailing factor controlling the emission energy, but for Tb-1.0 phase the structural effect becomes dominant. On the other hand, the Ba substitution seems to remarkably enhance the lattice covalency. The phase with the highest Ba loading fluoresces at the longest wavelength, despite having the largest $\langle d_{Ce-O} \rangle$.

In this study, we made attempts to prepare Ce^{3+} phosphors analogous to LSA:Ce^{3+} by isovalent substitution approaches, where the successful formation of each solid solution depends heavily on the geometric compatibility. An interesting finding is that the substitution in LSA structure is more restrictive when the substituent cation is smaller in size than the cation being replaced. Note that the solubilities of B and Ca are far below 50% in contrast to the complete solubility attained by the larger cations Ga and Ba. To explain this, it is instructive to consider the lattice stability of the basis composition LSA:Ce^{3+} first. The tetrahedral Al−O bond length in LSA:Ce^{3+} (1.726 Å) is somewhat shorter than the typical values close to 1.75 Å observed in similar aluminates.[39] For comparison, the Al−O distance in $EuSr_2AlO_5$ is 1.753 Å, and the 4-coordinate ionic radii for Al^{3+} and O^{2-} add to 1.79 Å. This structural aspect suggests that the AlO_4 tetrahedra in LSA:Ce^{3+} are under considerable chemical pressure. Further implied is that LSA:Ce^{3+} should be quite reluctant to any substitution that requires the contraction of internal AlO_4 blocks, as is the case of Ca and B. Tb and Gd are smaller than La but by a small margin, and moreover their substitutions take place at distances from AlO_4 units, so that they are not disfavored. On the other hand, Ba or Ga substitutions elongate the Al−O bonds toward the normal range, and will increase the lattice stabilization.

The rather short Al−O bond in LSA:Ce^{3+} is related also with the frequent occurrence of a competing phase $LaSrAlO_4$ (tetragonal, space group $I4/mmm$),[40] during the substitution reactions. The Ruddlesden−Popper $LaSrAlO_4$ provides octahedral cavities that Al^{3+} will readily occupy and is thus a phase that competes with LSA. The LSA:Ce^{3+} structure itself has a sufficient lattice stability that disallows the formation of $LaSrAlO_4$, provided the exact cation mixing ratio. However, the

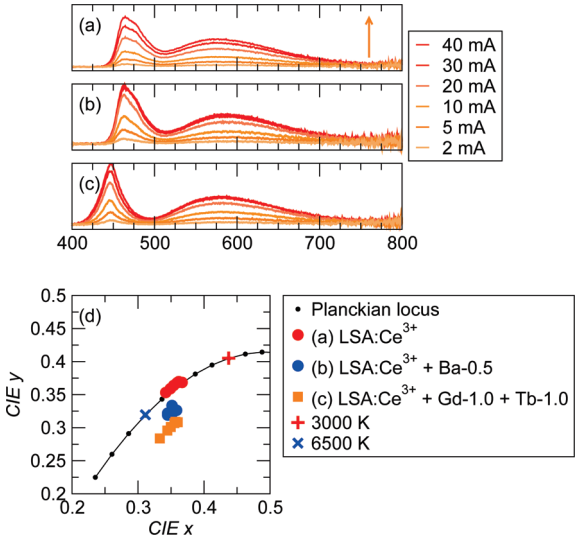

Figure 12. Luminescence of the InGaN LED + phosphor under different forward bias currents: (a) LSA:Ce^{3+} + InGaN LED (460 nm), (b) LSA:Ce^{3+} + Ba-0.5 + InGaN LED (460 nm), and (c) LSA:Ce^{3+} + Gd-1.0 + Tb-1.0 + InGaN LED (450 nm). (d) CIE chromatic coordinates of the device under different forward bias currents. The Planckian locus line and the points corresponding to color temperatures of 3000 and 6500 K are indicated.

Table 8. Optical Properties of the White LEDs Fabricated Using Various Phosphor Combinations with Blue LEDs: Combination A is LSA:Ce^{3+} + Ba-0.5 + InGaN LED (460 nm), and Combination B is LSA:Ce^{3+} + Gd-1.0 + Tb-1.0 + InGaN LED (450 nm)

phosphor	R_a	CIE x	CIE y	color temperature (K)	efficacy (lm/W)
LSA:Ce^{3+}	80−82	0.342−0.366	0.353−0.368	4340−5122	10−17
Combination A	78−80	0.344−0.358	0.319−0.333	4322−4885	7−13
Combination B	81−85	0.333−0.360	0.283−0.308	4070−5411	6−13

unfavorably short Al−O bonds in LSA:Ce^{3+} causes an instability to any substitution that critically disturbs the structural and/or electronic environments around AlO_4 tetrahedra, eventually leading to phase equilibria between $LaSrAlO_4$ and the aimed substitution phase. It is noteworthy that the Ruddlesden−Popper impurity is suppressed in the B-0.1 sample, which is attributed to the coordination preference of trivalent boron ions. The very small B^{3+} cation is stabilized usually in three- or four-coordinate environments,[41] but not in 6-fold coordination. Therefore in the compositional space of La−Sr−B−Al−O, the formation of $LaSr(B,Al)O_4$-type phases can be disregarded, let alone $LaSrBO_4$. Our observation indicates that the coordination of Al^{3+} ion is effectively regulated by homogeneous mixing with 10%B. This finding can be applicable to various solid-state preparations where these impurity problems occur.

Performance of Prototype White LEDs. White LED lamp devices were fabricated using various phosphor combinations together with InGaN LEDs (λ_{max} = 450 and 460 nm). The phosphors obtained in this study are all derived from LSA:Ce^{3+} and are excited by similar energies of 450 nm. Therefore, they can be blended to broaden the practical emission range without compromising on emission intensity. Through systematic trials, we found it useful to prepare the phosphor components for the LED device, in the following mixtures, LSA:Ce^{3+} + Ba-0.5 (50:50 wt %) and LSA:Ce^{3+} + Gd-1.0 + Tb-1.0 (33:33:33 wt%). Figure 12 shows the electroluminescence spectra measured for several selected devices under different forward-bias currents in the range of 2−40 mA, along with the Commission International de l'Eclairage (CIE) chromaticity. The measured optical properties of those white LED lamps are also summarized in Table 8. All those LED devices from the composite phosphors showed higher R_a values than those prepared with YAG:Ce^{3+} in a similar manner. Although the color properties of the present devices, expressed as CIE chromaticity, are somewhat poorer than anticipated, we expect further improvements will be made by variation of the phosphor blending, as well as with manipulation of individual phosphor compositions.

Summary and Conclusions

Yellow-emitting Ce^{3+} phosphors $La_{0.975-x}Ln_xCe_{0.025}Sr_2AlO_5$ (Ln = Gd, Tb), $La_{0.975}Ce_{0.025}Sr_{2-2y}AE_{2y}AlO_5$ (AE = Ca, Ba), and $La_{0.975}Ce_{0.025}Sr_2Al_{1-z}T_zO_5$ (T = B, Ga) were prepared on the basis of a parent composition $La_{0.975}Ce_{0.025}Sr_2AlO_5$ (LSA:Ce^{3+}). In all the above solid solution phases, the activator Ce^{3+} ion is stabilized in the distorted square antiprism of oxide, and the 5d states split into five different levels. As shown by the Rietveld analyses used in conjunction with photoluminescence measurements, the Ce 5d → 4f emission energies of the above phosphors vary across a range, in accordance with the change of Ce−O distances and the associated crystal field splitting. In particular, the Gd-substitution for La turns out to be the most useful for increasing the crystal field splitting, and thus for enhancing the red component of emission. In Tb- or Ba-substitutions, lattice covalency plays an additional role in influencing the emission energy. Phase stabilities of the above LSA:Ce^{3+}-based substitution products depend on the structural tolerance of internal tetrahedral blocks. The parent LSA:Ce^{3+} structure contains short Al−O bonds that are quite resistant to further compression. Consequently the substitutions of smaller cations B^{3+} (for Al^{3+}) or Ca^{2+} (for Sr^{2+}) can occur only to a limited extent. On the other hand, it is notable that a few percent substitution of B for Al can effectively suppress the formation of a competing phase $LaSrAlO_4$. Using the phosphors prepared in this study, prototype white LED lamps were successfully fabricated using InGaN LEDs. From preliminary examination, we found two phosphor formulations (LSA:Ce^{3+} + Ba-0.5 and LSA:Ce^{3+} + Gd-1.0 + Tb-1.0), which lead to improved R_a values of the lamp device.

Acknowledgment. The National Science Foundation is gratefully acknowledged for the use of MRSEC facilities (DMR05-20415). We thank Dr. Serena Corr for helpful suggestions.

(39) Smith, J. V.; Bailey, S. W. *Acta Crystallogr.* **1963**, *16*, 801.
(40) Byszewski, P.; Diduszko, R.; Wojcik, J.; Pajaczkowska, A. *Cryst. Prop. Prep.* **1991**, *36*, 553.
(41) Davidson, M. G.; Hughes, A. K.; Marder, T. B.; Wade, K. Contemporary Boron Chemistry; Royal Society of Chemistry: London, 2000.